Microstructures for lowering the quarter wavelength resonance frequency of a hard-backed rigid-porous layer

Keith Attenborough, keith.attenborough@open.ac.uk
Engineering and Innovation, The Open University, Milton Keynes, MK7 6AA, UK

Abstract

The frequency of the quarter wavelength resonance in the sound absorption spectra due to a thin hard-backed rigid-porous layer can be influenced by the design of its microstructure as well as its thickness. Microstructures considered include parallel arrays of identical cylindrical, slit-like or rectangular pores with deep sub-wavelength cross sections inclined to the surface normal, cylindrical annular pores, slits with log-normal width distributions, slits with cross sections that vary in a sinusoidal manner and slits with two distinct widths (dual porosity). Formulae that predict the bulk acoustical properties due to these microstructures are presented and used to explore the extent to which specific microstructures could be used separately or in combination to improve low-frequency absorption. Predicted normal incidence absorption coefficient spectra are compared using microstructural dimensions that would be feasible for 3D printing. The most effective microstructures are predicted to be slits with sinusoidally-varying widths, or with two distinct widths, inclined to the surface normal at 70°. The quarter wavelength layer resonances predicted in absorption coefficient spectra using these microstructures are comparable with those predicted for layers of the same thickness and bulk porosity having cylindrical pores with dead-end branches.

Keywords: porous absorber, slit microstructures, quarter-wavelength resonance

1. Introduction

Thin lightweight sound absorbing layers are required for several applications, in vehicles for example. A common problem for thin porous absorbers, which depend on viscous friction and thermal exchanges in pores, is that the low frequency absorption is poor. Low-frequency tuned absorption can be provided by Helmholtz resonators but these, along with many metamaterial alternatives to traditional porous absorbers, may be too bulky. Sound absorbing metallic foams, made by fusing metal spheres together and then perforating the fused sphere assemblies, are of interest because of their rigidity, lightness, thermal conductivity and their low production cost compared to open-cell metallic foams [1]. A hard-backed 0.0264 m thick perforated metallic foam has a narrow quarter wavelength layer resonance with a peak normal incidence absorption coefficient of 1 at 1 kHz and has estimated bulk parameters of porosity 0.283, flow resistivity 8.4 kPa s m^{-2} and tortuosity 5.54 [1].

By using 3D-printing technology, it is possible to manufacture rigid-porous sound absorbing materials with precisely specified microstructures. The average measured absorption coefficient spectrum of a 44.4 mm diameter hard-backed 0.03 m thick 3D printed cylindrical sample with overall porosity 0.234, incorporating cylindrical main pores of diameter 3.2 mm normal to the surface and cylindrical dead-end pores of diameter 1.3 mm normal to the main pores, has a broad quarter-wavelength layer resonance peak with magnitude 0.9 near 2.2 kHz [2]. A proposed 0.03 m thick layer with such a dead-end pore microstructure is predicted to result in a narrow absorption coefficient peak of magnitude 0.85 at 1.25 kHz. Another dead-end-pore microstructure design for a 0.035 m thick layer is predicted to give a narrow absorption coefficient peak with magnitude 0.65 at 0.65 kHz [2]. It has been found that hard-backed layers with cylindrical annular pores yield higher absorption than layers with the same thickness but with open cylindrical pores [3]. The measured absorption coefficient peak magnitude of 0.55 near 3.5 kHz for a 0.025 m thick sample containing 2 mm diameter cylindrical pores and with porosity 0.26 is increased to 0.95 near 3 kHz by inserting cylindrical

rods into the open pores thereby creating annular pores of width 0.25 mm and reducing the bulk porosity to 0.11 [3].

Another simple microstructure is an array of uniform identical parallel-sided narrow channels or slits parallel to the surface normal. Two ways of improving the low-frequency absorption of thin porous layers containing parallel uniform slits have been investigated. One involves varying the width of the slits in a sinusoidal manner [4]. The other is to introduce two arrays of slits at right angles to each other, one with relatively large and the other with relatively small widths [5].

Analytical models for the acoustical properties of cylindrical, annular and slit microstructures are outlined and extended to allow for inclination of the pores to the surface normal since this increases the bulk tortuosity and thereby lowers the quarter wavelength resonance frequency. The extended models are used to investigate the extent to which each form of microstructure either separately or in combination could be used to improve low-frequency absorption of a thin hard-backed layer. Numerical comparisons use microstructure dimensions on the order of those of metallic foams [1] or of those that have been used elsewhere [2-5]. The chosen dimensions are within the resolution of commonly-available 3D-printers (0.1 mm at present).

2. Models for uniform identical pores

2.1 Parallel identical uniform pores

If the complex density in a (single) uniform pore of arbitrary shape is written

$$\rho(\omega) = \rho_0 / H(\lambda) \tag{1}$$

where ω is the angular frequency and λ is a dimensionless parameter, then the complex compressibility [6-8] is

$$C(\omega) = (\gamma P_0)^{-1}[\gamma - (\gamma - 1)H(\lambda\sqrt{(N_{PR})})] \tag{2}$$

where $(\gamma P_0)^{-1} = (\rho_0 c_0^2)^{-1}$ is the adiabatic compressibility of air, P_0 is atmospheric pressure and γ is the ratio of specific heats.

Expressions for $H(\lambda)$ and λ corresponding to various pore cross sections are listed in Table 1 in which $\nu = \mu/\rho_0$, where μ is the dynamic viscosity coefficient, ρ_0 is the (equilibrium) density of air, c_0 is the adiabatic sound speed in air and time dependence $\exp(-i\omega t)$ is understood.

Table 1 Complex density functions for four pore shapes

Pore Shape	λ	$H(\lambda)$
slit (width $2b$)	$b\sqrt{(\omega/\nu)}$	$1 - \tanh(\lambda\sqrt{-i})/(\lambda\sqrt{-i})$
cylinder (radius a)	$a\sqrt{(\omega/\nu)}$	$1 - (2/\lambda\sqrt{i})J_1(\lambda\sqrt{i})/J_0(\lambda\sqrt{i})$
equilateral triangle (side d)	$(d\sqrt{3}/4)\sqrt{(\omega/\nu)}$	$1 - 3\coth(\lambda\sqrt{-i})/(\lambda\sqrt{-i}) + 3i/\lambda^2$
rectangle (sides $2a$,$2b$)	$\frac{2ab}{\pi\sqrt{(a^2+b^2)}}\sqrt{(\omega/\nu)}$	$\frac{-4i\omega}{\mu a^2 b^2}\sum_{k=0}^{\infty}\sum_{l=0}^{\infty}\left\{\alpha_k^2\beta_l^2\left[\alpha_k^2+\beta_l^2-\left(\frac{i\omega}{\mu}\right)\right]^{-1}\right\}$, $\alpha_k = \left(k+\frac{1}{2}\right)\left(\frac{\pi}{a}\right)$, $\beta_l = \left(l+\frac{1}{2}\right)\left(\frac{\pi}{b}\right)$

The dimensionless parameter for an arbitrarily-shaped pore, λ can be related to the (steady) flow resistivity (R_S) of the bulk material of porosity Ω through the Kozeny-Carman formula [9],

$$R_s = \frac{2\mu T s_0}{\Omega r_h^{\,2}}, \tag{3}$$

where the hydraulic radius, $r_h = \frac{\text{'wetted' area}}{\text{perimeter}}$, s_0 is a steady flow shape factor and T is tortuosity, defined as the square of the increase in path length per unit thickness of material due to deviations of the steady-flow path from a straight line, and Ω is porosity.
Expressions for r_h and s_0 are listed in Table 2.

Table 2 Hydraulic radius and steady flow shape factors for four pore shapes [9]

shape	r_h	s_0
slit, width $2b$	b	1.5
cylinder, radius a	$\frac{a}{2}$	1
equilateral triangle, side d	$\frac{d}{4\sqrt{3}}$	$\frac{5}{6}$
square, side $2a$	$\frac{a}{2}$	0.89

If the pores are inclined at angle θ to the surface normal, then [10]

$$T(\theta) = 1/\cos^2(\theta) \tag{4}$$

The complex density ($\rho_b(\omega)$) and complex compressibility ($C_b(\omega)$) for the bulk material are calculated from those for an individual pore using equations (5a,b):

$$\rho_b(\omega) = (T/\Omega)\rho(\omega), \;\; C_b(\omega) = \Omega C(\omega) \tag{5a,b}$$

The bulk propagation constant ($k(\omega)$) and relative characteristic impedance ($Z_c(\omega)$) of the porous material consisting parallel slits of width $2b$ and edge-to-edge separation $b(1 - \Omega)/\Omega$ may be calculated from equations (6a,b).

$$k(\omega) = \omega[\rho_b(\omega)C_b(\omega)]^{0.5}, \; Z_c(\omega) = (\rho_0 c_0^2)^{-1}[\rho_b(\omega)/C_b(\omega)]^{0.5} \tag{6a,b}$$

The surface impedance of a hard-backed porous layer of thickness d is,

$$Z(d) = Z_c \coth(-ikd). \tag{7}$$

The plane wave reflection coefficient, $R(d)$, and normal incidence absorption coefficient, $\alpha(d)$, for a hard -backed porous layer are given by equations (8a,b):

$$R(d) = \frac{\rho_0 c_0 - Z(d)}{\rho_0 c_0 + Z(d)}, \qquad \alpha(d) = 1 - \left|\left(R(d)\right)^2\right| \tag{8a,b}$$

respectively.
Using the values in Table 2 with equation (3), if a medium contains slits of width $2b$, $r_h = b$, $s_0 = 1.5$, and $R_s = 3\mu T/\Omega b^2$. If a medium contains cylindrical pores of radius a, $r_h = a/2$, $s_0 = 1$, and $R_c = 8\mu T/\Omega a^2$. For a given porosity and tortuosity, a layer with cylindrical pores of radius a will have 8/3 times the flow resistivity of a medium containing slits with semi-width a. A medium containing square pores of side $2a$ will have 0.89 of the flow resistivity of one containing cylindrical pores with radius a.

2.2 Cylindrical annular pores

Exact equations for a cylindrical annular pore involve cylindrical Bessel functions, as do those for an open cylindrical pore [3]. However, it has been shown [3] that, a semi-phenomenological model for an arbitrary pore microstructure, the Johnson-Champoux-Allard-Lafarge (JCAL) model [11,12], enables sufficiently accurate predictions of the acoustical properties of a layer

containing cylindrical annular pores normal to the surface. In general, the JCAL model introduces viscous and thermal permeabilities, viscous and thermal characteristic lengths, porosity and tortuosity. For cylindrical annular pores, the viscous and thermal characteristic lengths are equal, as are the viscous and thermal permeabilities. Calculations for annular pores with outer radius *R*, ratio *r* of outer-to-inner radii and centre-to-centre spacing *L* are made using equations (9) and (10).

$$\rho_b(\omega) = T\rho_0\left[1+\frac{iR_A\Omega}{\omega\rho_0 T}G(R,r,L,T)\right], \tag{9}$$

where $G(R,r,L,T) = \sqrt{\left(1-\frac{4iT\eta\rho_0\omega}{R_A{}^2R^2(1-r)^2\Omega^2}\right)}$, $\Omega = \pi R^2(1-r^2)/L^2$, $R_A = \frac{8T\eta}{\Omega R^2 Y(r)}$,

$$Y(r) = 1 + r^2 - (1-r^2)/ln(1/r)$$

and

$$C_b(\omega) = (\gamma P_0)^{-1}\left[\gamma-(\gamma-1)\left[1+\frac{iR_A\Omega}{\omega\rho_0 TN_{PR}}G'(R,r,L,T)\right]^{-1}\right] \tag{10},$$

where $G'(R,r,L,T) = \sqrt{\left(1-\frac{4iT\eta\rho_0\omega N_{PR}}{R_A{}^2R^2(1-r)^2\Omega^2}\right)}$.

R_A represents the flow resistivity of a material with parallel cylindrical annular pores.

By using equation (4) with equations (9) and (10), the original development [3] is extended to allow for inclination of annular pores to the surface normal.

2.3 Log-normal distributions of slit widths

The viscosity correction function for a log-normal distribution of uniform slit widths [13 – 17] is

$$F_{sd} = \frac{(-i\omega\mu\rho_0)}{\Omega R_s}\frac{\int_0^\infty b^{-1}e(b)\tanh(\lambda_s\sqrt{-i})db}{\int_0^\infty e(b)[1-\frac{\tanh(\lambda_s\sqrt{-i})}{(\lambda_s\sqrt{-i})}]db} \tag{11}$$

where $\int_0^\infty e(b)db = \int_{-\infty}^\infty f(\phi)d\phi$, $f(\phi) = \frac{1}{\sigma\sqrt{2\pi}}\exp[-(\phi-\phi_a)^2/2\sigma^2]$, $b = 2^{-\phi}$, $b_a = 2^{-\phi_a}$ and σ is the standard deviation of the pore size distribution in ϕ units. b_a represents the mean pore semi-width, related to the median pore semi-width, b_m, by $b_a = b_m\, e^{\sigma\log 2}$.

The flow resistivity for a log-normal distribution of uniform slits is $R_s = [\frac{3\mu}{\Omega b_a{}^2}]e^{-2(\sigma\ln 2)^2}$.

The pore and bulk complex densities are calculated from

$$\rho_{pd}(\omega) = \Omega\rho_0\left[1+\frac{iR_S\Omega}{\omega\rho_0 T}F_{sd}\right] = (\Omega/T)\rho_b(\omega). \tag{12}$$

Hence, using Stinson's relationship [6], the bulk complex compressibility is,

$$C_b(\omega) = \Omega(\gamma P_0)^{-1}\left[\gamma-(\gamma-1)\left(\rho_0/\rho_{pd}\left(\omega\sqrt{N_{\mathrm{Pr}}}\right)\right)\right]. \tag{13}$$

The numerical integration in equation (11) is avoided by Padé approximations [15-17].

For a medium consisting of identical uniform or non-uniform tortuous slits, equation (12) may be rewritten as

$$\rho_b(\omega) = (T\rho_0/\Omega)[1 + F(\varepsilon)/(T\varepsilon^2)] \tag{14}$$

where $\varepsilon = \lambda\sqrt{(-i)}$ and $F(\varepsilon)$ is the viscosity correction function (11) expressed in terms of ε.

Low- and high-frequency asymptotes for the viscosity correction function are

$$F(\varepsilon) = 1 + \theta_1\varepsilon^2 + O(\varepsilon^4), \quad \varepsilon \to 0 \tag{15}$$

and

$$F(\varepsilon) = \theta_2\varepsilon + O(1), \quad \varepsilon \to \infty. \tag{16}$$

Hence, a two-parameter Padé approximation for the viscosity correction function is [15- 17]

$$F(\varepsilon) = \frac{1 + a_1\varepsilon + a_2\varepsilon^2}{1 + b_1\varepsilon}, \tag{17}$$

where $a_1 = \theta_1/\theta_2$, $a_2 = \theta_1$ and $b_1 = a_1$.

For uniform slit-like pores, $\theta_1 = \frac{6}{5}e^{4\xi} - 1$ and $\theta_2 = \frac{1}{\sqrt{3}}e^{\frac{3}{2}\xi}$, where $\xi = (\sigma \ln 2)^2$.

For non-uniform parallel slit-like pores with a log-normal variation in widths [17], $\theta_1 = 1/5$, $\theta_2 = \frac{1}{\sqrt{3}}e^{-\frac{1}{2}\xi^2}$ and the flow resistivity is $R_s = [\frac{3\mu}{\Omega b_a^2}]e^{-6(\sigma \ln 2)^2}$. Inclination of pores to the surface normal is included through equations (3) and (4).

2.4 Slits with sinusoidal width variation

Figure 1 shows a variable-width channel of maximum semi-width b with 'mirror-image' sinusoidal-sides represented by

$$y_1(x) = 2b - a\cos(2\pi bx/X)$$
$$y_2(x) = a\cos(2\pi bx/X), \tag{18a, b}$$

where a is the amplitude and X is the wavelength of the sinusoidal variation.

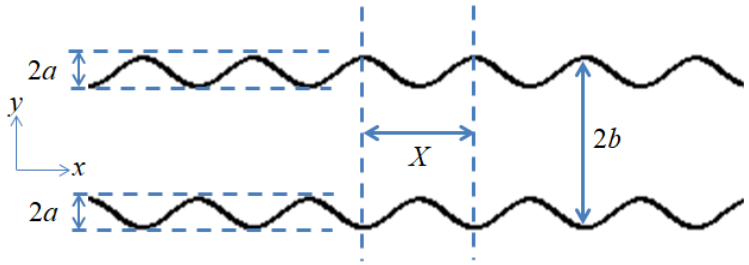

Figure 1 Cross section of a slit with a sinusoidally-varying width; maximum semi-width b and 'mirror-image' sinusoidal sides, amplitude a and wavelength X.

It has been shown [4] that, if $a/2b \leq 0.1$ and $X >> a$, the effective tortuosity is

$$T(a, X) = 1 + \left[\frac{e^{\frac{2\pi b}{X}} + 1}{e^{\frac{2\pi b}{X}} - 1}\right]\left(\frac{a}{2b}\right)^2\left(\frac{2\pi b}{X}\right), \tag{19}$$

and the effective flow resistivity is

$$R(b, a, X) = \left(\frac{3\mu}{b^2}\right)\left\{\left[\frac{2\left(\frac{a}{2b}\right)^2 + 1}{\left(1 - 4\left(\frac{a}{2b}\right)^2\right)^{2.5}} - \frac{1}{\left(1 - 2\left(\frac{a}{2b}\right)\right)^3}\right]\frac{2e^{-\frac{2b}{5X}}}{1 + e^{-\frac{2b}{5X}}} + \frac{1}{\left(1 - 2\left(\frac{a}{2b}\right)\right)^3}\right\}. \tag{20}$$

It has been shown numerically in [4], that, as the sinusoidal width variation becomes negligible, the predictions approach those for uniform slits parallel to the surface normal. Nevertheless, the development pursued in [4] uses the JCAL formulation [11,12]. Instead, the calculations presented here substitute for $T = T(\mathrm{a}, X)$ and $R_S = R(b, a, X)$ in equations (1), (2) and (5 - 8).

Furthermore, equation (19) is extended to allow for slits with sinusoidal width variation inclined at θ to the surface normal by using

$$T(a, X, \theta) = T(\theta) + (T(a, X) - 1) \quad . \tag{21}$$

This possibility was not considered in [4] which was aimed at the design of perforated micro-slit absorbers rather than bulk absorbers.

2.5 Dual porosity slits

Expressions for the effective complex density, ρ_{dp}, and effective complex compressibility, C_{dp}, of a medium containing meso-slits of semi-width b_{me} with edge-to-edge separation of $b_{me}(1 - \Omega_{\mathrm{me}})/\Omega_{\mathrm{me}}$ where Ω_{me} represents the porosity of meso-slits, connected to which, at right angles through the solid strips separating the meso-slits, are parallel micro-slits of semi-width b_{mi} with edge-to-edge separation of $b_{mi}(1 - \Omega_{\mathrm{mi}})/\Omega_{\mathrm{mi}}$, where Ω_{mi} represents the porosity of micro-slits are [5, 17]:

$$\rho_{dp}(\omega) = \left[\frac{1}{\rho_{me}(\omega)} + \frac{(1-\Omega_{me})}{\rho_{mi}(\omega)}\right]^{-1} \tag{22}$$

$$C_{dp}(\omega) = C_{me}(\omega) + (1 - \Omega_{me})C_{mi}(\omega). \tag{23}$$

The complex density and compressibility for each type of slit are calculated from the expressions for uniform slit-like pores.

These expressions are extended to allow for inclination of both types of slits to the surface normal by using equation (4). This possibility was not considered in [5].

3. Improving low frequency absorption

3.1 Identical parallel pores

Figures 2(a) and (b) compare predictions of normal incidence absorption coefficient spectra for a 3-cm thick hard-backed layers of porosity 0.25 containing (a) 2 mm diameter parallel identical cylindrical pores or (b) 2 mm wide parallel identical uniform slits, inclined at angles of 0°, 45° and 70° to the surface normal. The respective values of flow resistivity, according to equation (3), are 0.483 kPa s m^{-2}, 0.965 kPa s m^{-2} and 4.13 kPa s m^{-2} for the cylindrical pores and 0.182 kPa s m^{-2}, 0.364 kPa s m^{-2}, and 1.56 kPa s m^{-2} for the slits. Higher flow resistivity values for the cylindrical pore microstructure than for slits mean that the predicted peak absorption coefficient magnitudes are higher and broader at the quarter-wavelength layer resonance.

Increasing the angle of inclination of the pores to the surface normal is predicted to increase the magnitudes of the quarter wavelength layer resonances and decrease their frequencies. This is a consequence of increased tortuosity and reduced sound speed in the layer. The angles of 0°, 45° and 70° to the surface normal correspond to tortuosity values of 1, 2 and 8.55 respectively. As remarked elsewhere [1], to a first approximation, and in accordance with the definition of tortuosity [10], increasing the tortuosity, T, increases the effective thickness of the layer by a factor of $\sqrt{T}$. An angle of inclination of 70° implies, approximately, a three-fold increase in effective layer thickness and, hence, a three-fold decrease in the quarter wavelength resonance frequency. For both pore shapes, changing the inclination of the slits from parallel

to the surface normal to 70° to the surface normal is predicted to reduce the quarter-wavelength resonance frequency from near 3 kHz to near 1 kHz.

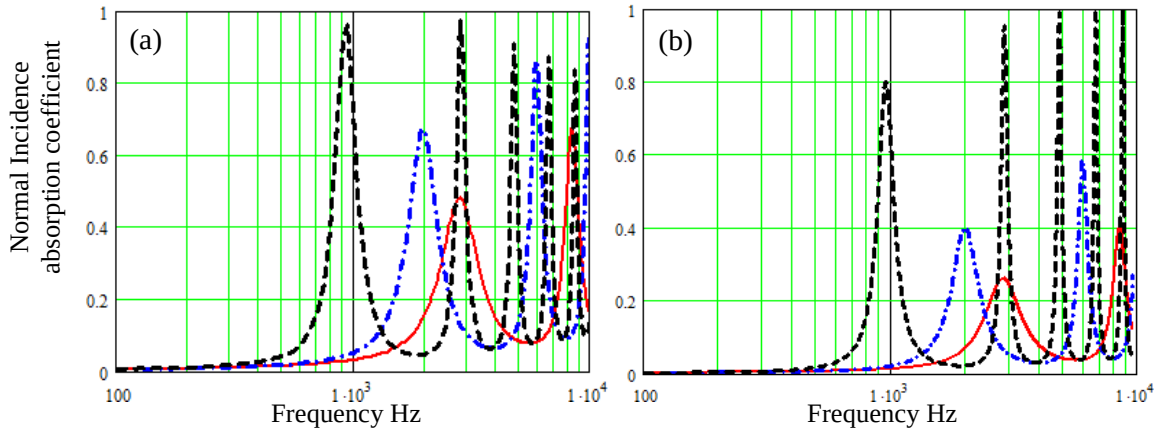

Figure 2 (color online) Predicted absorption coefficient spectra for 0.03 m thick rigid-porous layers with porosity 0.3 containing parallel uniform identical pores at angles to the surface normal of 0° (continuous red lines), 45° (dash-dot blue lines) and 70° (broken black lines): (a) cylindrical pores radius 1 mm and (b) slit pores width 2 mm.

According to equation (3), a layer with porosity 0.25 containing square pores of side 2 mm parallel to the surface normal has a flow resistivity of 0.432 kPa s m^{-2} compared with 0.182 kPa s m^{-2} for 2 mm wide slits. As shown in Figure 3, the higher flow resistivity is predicted to lead to a higher magnitude of the quarter-wavelength layer resonance peak for square pores than for slits.

It has been shown analytically [3,5] that the complex density function, $H(\lambda)$, for rectangular pores with sides $2a$ and $2b$ (see Table 1) reduces to that for slit pores of width $2b$ as $a \rightarrow \infty$. Figure 3 indicates that predicted rectangular and slit-pore absorption coefficient spectra are numerically identical when $a \geq 4b$.

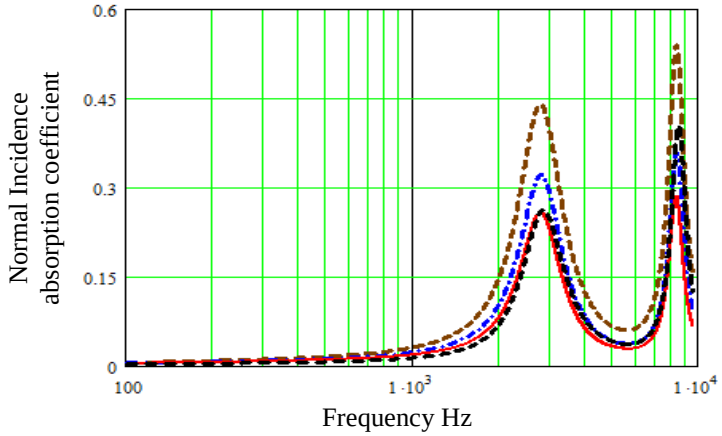

Figure 3 (color online) Absorption coefficient spectra predicted for a 0.03 m thick hard-backed rigid-porous layer with porosity 0.3 containing (normal to the surface) parallel 2 mm side identical square pores (broken brown line), 2 mm wide slit pores (continuous red line) and rectangular pores with longer sides of 4 mm (dash-dot blue line) and 8 mm (broken black line).

3.2 Annular pores

Figure 4 compares predicted absorption spectra for 0.03 m thick hard-backed rigid-porous layers with porosity 0.325 containing cylindrical pores (radius 1 mm) and cylindrical annular pores (outer radius 1 mm, radius ratio 0.325) either parallel to the surface normal or inclined at

70° to the surface normal. The chosen parameter values are similar to those of a measured sample and a linear frequency axis is used to correspond with that used in [3].

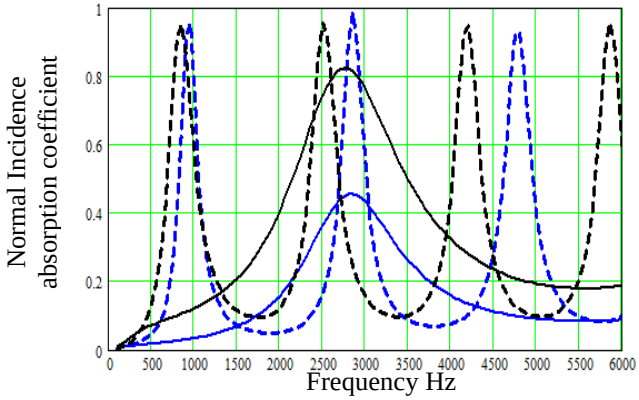

Figure 4 (color online) Predicted absorption coefficient spectra for a 0.03 m thick hard-backed rigid-porous layers with bulk porosity 0.325 containing parallel identical 1 mm radius cylindrical pores normal to the surface (continuous blue line) and at 70° to the surface normal (broken blue line). Also shown are predictions for cylindrical annular pores outer radius 1 mm, radius ratio 2/3, normal to the surface (continuous black line) and at 70° to the surface normal (broken black line).

The predicted absorption coefficient spectrum for cylindrical pores normal to the surface is slightly different from that in Fig. 2(a) since the porosity is slightly larger. The annular pore microstructure is predicted to result in a larger and broader quarter wavelength resonance absorption peak than predicted for cylindrical pores with the same (outer) radius without changing the frequency which is near 2.75 kHz. Inclining annular pores is predicted to offer only a marginal improvement over the predicted result of inclining cylindrical pores of the same (outer) radius.

3.3 Log-normal width distributions

Figure 5 shows a log-normal distribution $f(\phi)$ of slit widths, with a median width of 2 mm and standard deviation of 0.5 ϕ-units. The smallest pore width, of the order of 0.5 mm, is within the current resolution (0.1 mm) of 3D printing.

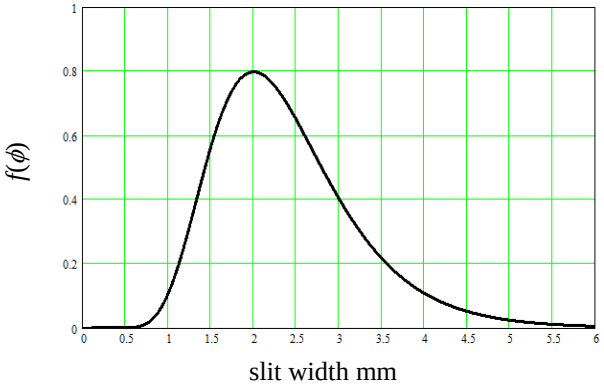

Figure 5 A log-normal slit width distribution $f(\phi)$ with median width 2 mm and standard deviation 0.5 ϕ-units.

Figure 6 (a) compares predicted absorption coefficient spectra for log-normal width distributions of uniform and non-uniform slits (median width 2 mm, standard deviation 0.5 ϕ-units) with that for identical slits of width 2 mm parallel to the surface normal. The width distributions of uniform and non-uniform slits are predicted to increase the flow resistivity from 0.109 kPa s m^{-2} to 0.138 kPa s m^{-2} and 0.223 kPa s m^{-2} respectively but do not influence the tortuosity.

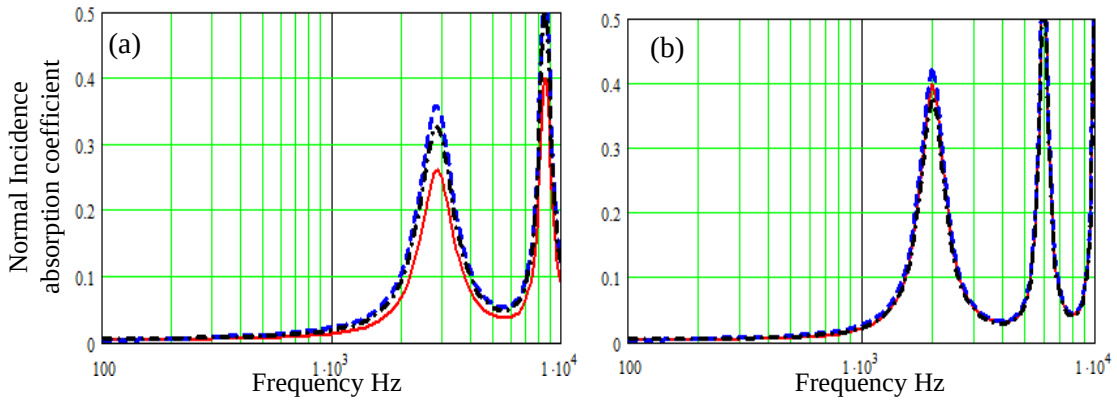

Figure 6 (color online) Absorption coefficient spectra predicted for a 3-cm thick hard-backed rigid porous layer with porosity 0.3 containing identical parallel 2 mm wide slits (continuous red lines), or log-normal width distributions (standard deviation 0.5 ϕ-units) of uniform slits (broken blue lines) or of non-uniform slits (dash-dot black lines) (a) parallel to the surface normal and (b) inclined at an angle of 45° to the surface normal.

When the slits are parallel to the surface normal, the width distributions are predicted to increase the magnitudes and broaden the layer resonances in the absorption coefficient spectra (Figure 6(a)) but not to affect their frequency. Figure 6(b) shows the corresponding predictions when the slits are inclined at 45°. The associated increase in tortuosity is predicted to lower the layer resonance frequency of the parallel identical slit layer and increase its magnitude, but more or less the same influence is predicted for microstructures involving log-normal width distributions. These predictions suggest that, if the median width is the same as for identical slits, there is little advantage in inclining slits with log-normal width distributions.

3.4 Slits with sinusoidal cross sections

In accordance with the approximation ($a/2b \leq 0.1$) used in obtaining equations (20) and (21) [4], and for the purposes of predicting the acoustical influences of sinusoidal variation in 2 mm slit widths, the amplitude of the variation, a, is fixed at $b/5$ i.e. 0.2 mm, which is within the current resolution (0.1 mm) of 3D printing. Figures 7(a) and (b) show the predicted influences of the wavelength of the width variation (X), as a fraction of the length of the slits (d), on the effective flow resistivity and tortuosity when the slits are parallel to the surface normal.

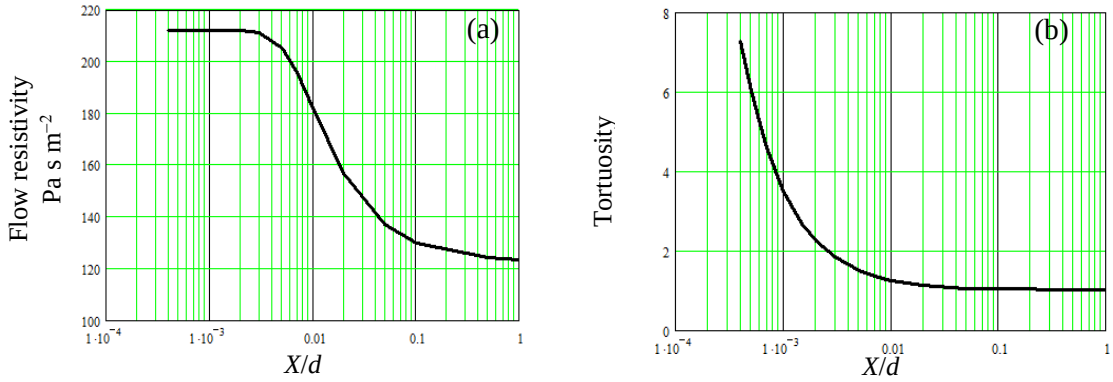

Figure 7 Predicted influence of the fractional wavelength X/d of sinusoidal variation (amplitude 0.2 mm) in pore width on (a) flow resistivity and (b) tortuosity according to equations (19) and (20).

The predicted influences on both flow resistivity and tortuosity are large if $0.1 > X/d > 0.005$. The predicted influence on tortuosity is very large when $X/d < 0.005$. However, in subsequent calculations, consistent with a 0.1 mm 3D-printing resolution limit, X is chosen to be 0.3 mm

i.e. 1/100 of the assumed layer thickness of 0.03 m. Also, this satisfies the approximation $X > a$, required in deriving equation (19).

Comparison of Figures 6(a) and 8 shows that a sinusoidal variation (amplitude 0.2 mm and wavelength 0.1 mm) in the width of slits parallel to the surface normal is predicted to increase the layer resonance absorption coefficient peak magnitude of a 0.03 m thick hard layer from 0.25 to 0.36 and to lower its frequency from 3 kHz to 2.4 kHz. A combination of sinusoidal variation in pore width (amplitude 0.2 mm, wavelength 0.03 mm) and 70° inclination of slits to the surface normal is predicted to give a quarter wavelength layer resonance absorption coefficient peak of 0.91 at 925 Hz.

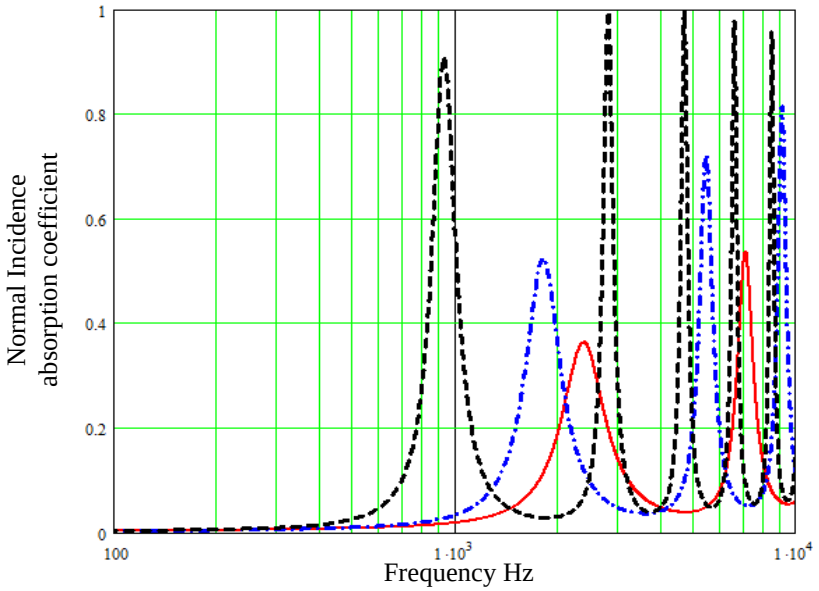

Figure 8 (color online) Predicted absorption coefficient spectra for a 3-cm thick hard-backed rigid porous layer containing parallel slits with a sinusoidal width variation (amplitude 0.2 mm, wavelength 0.024 mm, outer width 2 mm, edge-to-edge spacing 2 mm) normal to the surface (solid red line), inclined at 45° (dash-dot blue line) and inclined at 70° (broken black line).

3.5 Dual porosity slits

The acoustical influence of a dual porosity slit microstructure is investigated by assuming a 3-cm thick hard-backed layer including 2 mm wide meso-slits with edge-to-edge spacing 8 mm, and, at right angles, 0.2 mm wide micro-slits with edge-to-edge spacing 1.4 mm. The micro-slit width of 0.2 mm, is within the resolution (0.1 mm) of 3D printing. The meso- and micro-porosities of 0.2 and 0.125 respectively are consistent with the bulk porosity of 0.3 used in the previous calculations. Predicted absorption spectra (Figure 9) indicate that, with slits normal to the surface, the 0.25 peak absorption at 3 kHz is increased to more than 0.75 at a slightly lower frequency by the dual porosity microstructure.

A broad absorption peak with a magnitude of 0.95 is predicted at 1800 Hz when slits in the dual porosity microstructure are inclined at 45° to the surface and a broad absorption peak with a magnitude of 0.85 is predicted at 850 Hz when slits in the dual porosity microstructure are inclined at 70° to the surface normal.

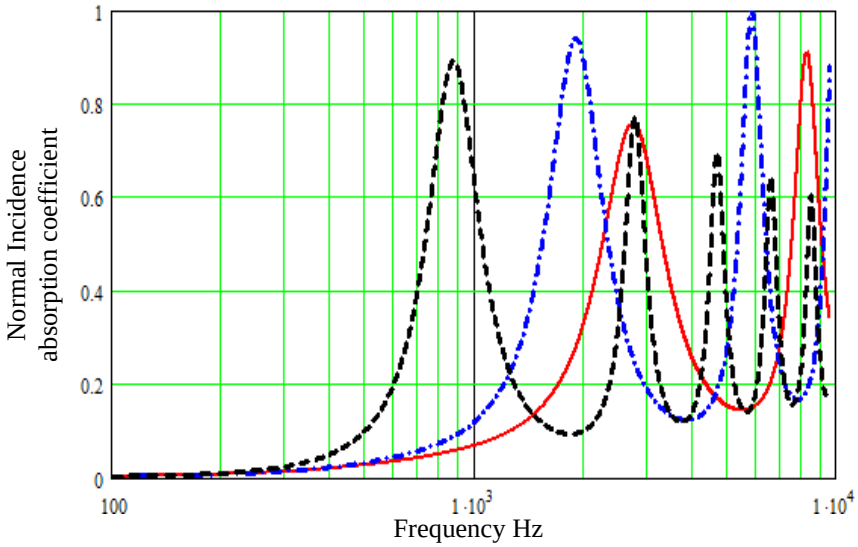

Figure 9 (color online) Predicted absorption coefficient spectra for a 3-cm thick hard-backed rigid-porous layer containing a microstructure of 2 mm wide meso-slits, edge-to-edge spacing 8 mm and 0.2 mm wide micro-slits, edge-to-edge spacing 1.4 mm, parallel to the surface normal (continuous red line) or at 45° to the surface (dash-dot blue line) or at 70° to the surface normal (broken black line).

3.6 Sound speeds

Figures 10(a), (b) and (c) show that, as well as increasing tortuosity, slits inclined with respect to the surface normal are predicted to reduce the sound speed normal to the surface within a rigid porous layer thereby increasing the effective depth of the layer. The predicted sound speeds reduce proportionately to the increase in $\sqrt{T}$.

When the slits are normal to the surface, sinusoidal variation in slit width is predicted to lead to a significant broadband reduction in sound speed (Figure 10(b)). The broader absorption peaks predicted for the dual porosity slit microstructures (Figure 9) are the result of greater predicted dispersion (Figure 10(c)) and, therefore, greater predicted attenuation of sound within a dual porosity slit-pore medium than predicted for the other slit configurations.

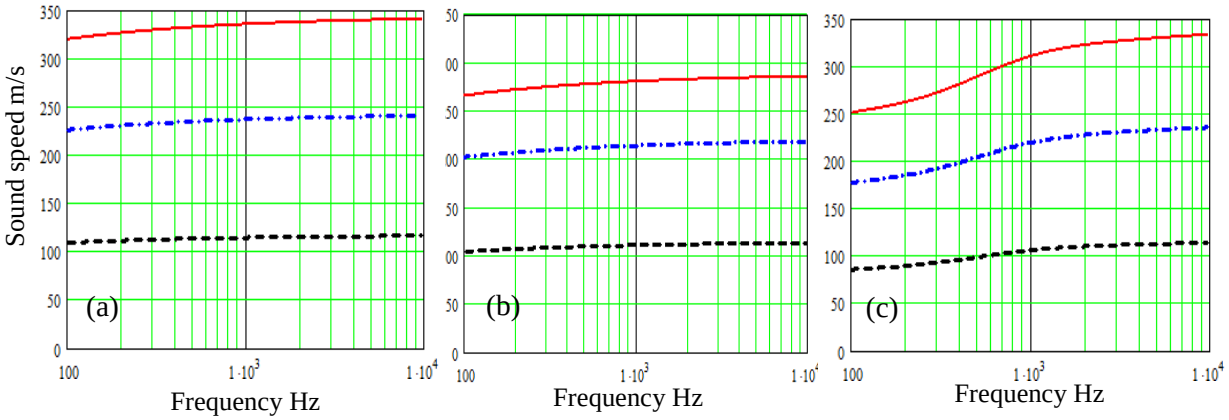

Figure 10 (color online) Predicted dispersion of sound in a rigid-porous medium (porosity 0.3) with slits inclined to the surface normal at 0° (continuous red lines), 45° (dash-dot blue lines) and 70° (broken black lines) assuming (a) uniform 2 mm wide slits (b) sinusoidally-varying widths, wavelength 0.3 mm, amplitude 0.2 mm (outer width 2 mm) and (c) dual-porosity with meso- (2mm wide, edge-to-edge spacing 8 mm) and micro-slits (0.2 mm wide, edge-to-edge spacing 1.4 mm).

4 Concluding Remarks

Sound absorption spectra have been calculated for hard-backed rigid-porous layers with several specified microstructures. Improvements to the low frequency absorption of the hard-backed layer containing uniform pores parallel to the surface normal are predicted if the pores are inclined to the surface normal, since this increases tortuosity and reduces sound speed normal to the surface, thereby lowering the frequencies of the quarter wavelength layer resonances and increasing their magnitudes, particularly if the flow resistivity is relatively low (~ 1 kPa s m^{-2}).

Although a significant improvement in normal incidence absorption of a 0.03 m thick hard-backed layer with 2 mm diameter open cylindrical pores parallel to the surface normal is predicted if the open pores are replaced by 1/3 mm wide cylindrical annular pores with outer radius 2 mm, much less improvement is predicted if the pores are inclined at 70° to the surface normal (see Figure 4).

Useful reductions in the quarter wavelength layer resonance frequency are predicted if the slits have sinusoidally-varying widths, or are arranged in a dual porosity microstructure as well as being inclined to the surface normal. The slit dimensions, spacing and layer thickness that have been used in this study are consistent with those considered in previous work [2 - 5] and give an indication of the potential for producing porous layers with slit-based microstructures using current 3D-printing technology.

Further reductions in the quarter wavelength layer resonance frequencies and greater magnitudes would be possible if 3D printing with a greater resolution than 0.1 mm were to be available. This would mean, for example, that sinusoidal width variations could have shorter wavelengths and slit widths could be reduced, thereby increasing flow resistivity. Nevertheless, the absorption coefficient spectra shown in Figures 8 and 9, predicted for 70° inclined slits with sinusoidally-varying widths or with dual porosity are comparable with those measured and predicted for 0.03 m thick absorbers with dead-end pore microstructures [2].

Acknowledgement

The idea of this paper was initiated by activities and communications associated with the EC COST network DENORMS.

References

[1] Chevillotte F, Perrot C, Panneton R. Microstructure based model for sound absorption predictions of perforated closed-cell metallic foams. J. Acoust. Soc. Am. 2010; 128: 1766 –76
[2] Leclaire P, Umnova O, Dupont T, Panneton R. Acoustical properties of air-saturated porous material with periodically distributed dead-end pores. J. Acoust. Soc. Am., 2015; 134: 1772 –82.
[3] Nori M, Venegas R. Sound propagation in porous materials with annular pores. J. Acoust. Soc. Am. 2017; 141: 4642 –51.
[4] Song SY, Yang XH, Xin FX, Ren SW, Lu TJ. Modeling of roughness effects on acoustic properties of micro-slits. J. Appl. Phys. D. 2017; 50: 235303.
[5] Ren SW, Meng H, Xin FX, Lu TJ. Sound Absorption Enhancement by Thin Multi-Slit Hybrid Structures. Chinese Physics Letters. 2015; 32: 014302.
[6] Stinson MR. The propagation of plane sound waves in narrow and wide circular tubes and generalisation to uniform tubes of arbitrary cross-sectional shape. J. Acoust. Soc. Am. 1991; 89: 550 –8.
[7] Champoux Y, Stinson MR. On acoustical models for sound propagation in rigid frame porous materials and the influence of shape factors, J. Acoust. Soc. Am. 1992; 92: 1120-31.

[8] Stinson MR, Champoux Y. Propagation of sound and the assignment of shape factors in model porous materials having simple pore geometries, J. Acoust. Soc. Am. 1992; 91: 685 – 95.
[9] Carman PC. Flow of gases through porous media. Butterworths. London. 1953.
[10] Zwikker C, Kosten CW. Sound Absorbing Materials. Elsevier. Amsterdam. 1949.
[11] Johnson DL, Koplik J, Dashen R. Theory of dynamic permeability and tortuosity in fluid-saturated porous media. J. Fluid Mech. 1987; 176: 379–402.
[12] Lafarge D, Lemarinier P, Allard JF, Tarnow V. Dynamic compressibility of air in porous structures at audible frequencies. J. Acoust. Soc. Am. 1997; 102: 1995–2006.
[13] Yamamoto T, Turgut A. Acoustic wave propagation through porous media with arbitrary pore size distributions. J. Acoust. Soc. Am. 1998; 83: 1744 –51.
[14] Attenborough K. Models for the acoustical properties of air-saturated granular media. Acta Acustica 1993; 1: 213 –226.
[15] Horoshenkov KV, Attenborough K, Chandler-Wilde SN. Padé approximants for the acoustical properties of rigid frame porous media with pore size distribution. J. Acoust. Soc. Am. 1998; 104: 1198 –1209.
[16] Horoshenkov KV, Swift MJ. The acoustic properties of granular materials with pore size distribution close to log-normal. J. Acoust. Soc. Am., 2001; 110: 2371 –78.
[17] Horoshenkov K, Groby JP, Dazel O. Asymptotic limits of some models for sound propagation in porous media and the assignment of the pore characteristic lengths. J. Acoust. Soc. Am. 2016; 139: 2463 –74.
[18] Olny X, Boutin C. Acoustic wave propagation in double porosity media. J. Acoust. Soc. Am. 2003; 114: 73 –89.